cient TiO_2 surface after the 120-min CO:O_2 exposure (Fig. 5) is likely lowering the activity of Au/TiO_2 even further, because the fully oxidized stoichiometric TiO_2 surface can no longer adsorb O_2 at 300 K (*13*). Oxidation of the TiO_2 surface during CO oxidation also provides direct evidence that the deactivation is not likely caused by encapsulation of Au clusters by reduced Ti suboxides as, for example, in the case of Pt/TiO_2(110) (*14*).

In order to better understand the role of O_2 in CO oxidation and in various O_2 pretreatments that are commonly applied to Au/TiO_2 catalysts to improve their activity (*15*), the clean TiO_2(110) surface (Fig. 6A) was exposed to O_2 at 2×10^{-8} Torr. After O_2 treatment, small islands randomly nucleated on TiO_2(110) and finally covered the entire surface (Fig. 6B). Low-energy electron diffraction (LEED) showed a (1×1) pattern indicating that the islands are growing pseudomorphically. XPS measurements of this rough TiO_2 surface after the O_2 treatment indicate that the surface is not significantly changed in chemical composition and thus is still slightly O-deficient. Recently, it was suggested that partially reduced Ti^{n+} ($n \leq 3$) ions can be formed in a vacuum-annealed and Ar^+-bombarded TiO_2(110) surface by annealing at 800 K and reoxidizing to TiO_2(110)-(1×1) terraces in an O_2 ambient of 7.5×10^{-8} Torr (*7*). A similar kind of oxidation of the reduced Ti^{n+} ions may occur during the O_2 treatment used here.

The influence of the O_2-exposed, rough TiO_2 surface on the sintering of the Au clusters during CO oxidation at 300 K is shown in Fig. 6, C and D. If we compare a CCT STM image of 0.25 ML Au on TiO_2(110)-(1×1) after deposition of Au at 300 K, annealing at 850 K for 2 min, and a subsequent O_2 exposure of 2×10^{-8} Torr at 650 K for 10 min (Fig. 6C) with one for which no O_2 treatment was made (Fig. 2A), the only difference is the general disorder of the TiO_2 surface. The cluster density and size distribution of the Au clusters are identical for both surfaces. Upon exposure of the rough Au/TiO_2(110) surface to CO:O_2 for 120 min at a total pressure of 10 Torr at 300 K, the cluster density and size distribution of the Au clusters remain unchanged (Fig. 6D). The Au/TiO_2(110) surface was oxidized after the high pressure CO:O_2 exposure (Fig. 4) and the cluster density of the TiO_2 clusters increased. The O_2-exposed, rough TiO_2 surface then prevents sintering of the Au clusters. Furthermore, a similar kind of atomically rough TiO_2 phase may be formed during the high-temperature reduction, calcination, and low-temperature reduction (HTR/C/LTR) procedure used on high–surface area Au/TiO_2 catalysts (*15*). After this treatment Au/TiO_2 catalysts exhibit a higher degree of resistance toward sintering of the Au clusters during CO oxidation at low temperatures (*15*).

These results indicate that the pronounced structure sensitivity of CO oxidation on Au/TiO_2 originates from quantum size effects associated with the supported Au clusters. The observed tailoring of the properties of small metal clusters by altering the cluster size and its support could prove to be universal for a variety of metals and will likely be quite useful in the design of nanostructured materials for catalytic applications.

References and Notes

1. D. R. Rainer, C. Xu, D. W. Goodman, *J. Mol. Catal. A Chem.* **119**, 307 (1997).
2. S. C. Street and D. W. Goodman, *The Chemical Physics of Solid Surfaces*, D. A. King and D. P. Woodruff, Eds. (Elsevier, Amsterdam, 1997), vol. 8, p. 375.
3. D. W. Goodman, *J. Phys. Chem. (Centennial Ed.)* **100**, 13090 (1996).
4. M. Haruta, *Catal. Catal. Today* **36**, 153 (1997).
5. H. Huber, D. McIntosh, G. A. Ozin, *Inorg. Chem.* **16**, 975 (1977).
6. M. Haruta *et al.*, *J. Catal.* **144**, 175 (1993).
7. G. R. Bamwenda, S. Tsubota, T. Nakamura, M. Haruta, *Catal. Lett.* **44**, 83 (1997).
8. The experiments were carried out in a combined elevated-pressure reactor–ultrahigh vacuum (UHV) system with a base pressure of 5×10^{-11} Torr equipped with a double-pass cylindrical mirror analyzer for Auger electron spectroscopy (AES) and XPS measurements, a quadrupole mass analyzer, and a UHV-STM (Omicron) [R. A. Campbell and D. W. Goodman, *Rev. Sci. Instrum.* **63**, 172 (1992)]. After preparation and characterization in the UHV chamber, the Au/TiO_2(110) model catalyst was transferred in situ into the reaction chamber through a double-stage, differentially pumped Teflon sliding seal. This arrangement facilitates elevated-pressure adsorption studies in the pressure range of 1×10^{-8} to 1×10^{3} Torr. A TiO_2(110) single crystal (Commercial Crystal Laboratories), an *n*-type semiconductor after cycles of Ar^+-ion bombardment and vacuum annealing at 700 to 1100 K, was found to be sufficiently conductive for electron spectroscopy and STM studies. This cleaning procedure produces a slightly oxygen-deficient surface with a well-ordered (1×1) surface as characterized by LEED and XPS measurements [J.-M. Pan, B. L. Maschhoff, U. Diebold, T. E. Madey, *J. Vac. Sci. Technol. A* **10**, 2470 (1992); L. Zhang, R. Persaud, T. E. Madey, *Phys. Rev. B* **56**, 10549 (1997)]. Gold clusters were evaporated onto the TiO_2(110) surface from a source containing high-purity Au wire wrapped around a W filament that was heated resistively. The Au flux was calibrated with a Re(0001) subtrate by using AES and STM as described (*13*). The Au coverage is reported in monolayers (ML), one ML corresponding to 1.387×10^{15} atoms per centimeter squared. After the Au deposition, the sample was annealed at 850 K for 2 min. The sample temperature was measured with a pyrometer (OMEGA OS3700), which was calibrated against a W-5% Re/W-26% Re thermocouple. Research-grade CO was further purified by storing at liquid N_2 temperatures; O_2 was used as received. The CO:O_2 (2:1) mixture was prepared separately before the adsorption experiments.
9. C. Xu, X. Lai, G. W. Zajac, D. W. Goodman, *Phys. Rev. B* **56**, 13464 (1997).
10. S. Pak, M. Valden, X. Lai, D. W. Goodman, in preparation.
11. N. D. S. Canning, D. Outka, R. J. Madix, *Surfactant Sci.* **141**, 240 (1984).
12. Y. Iizuka *et al.*, *Catal. Today* **36**, 115 (1997).
13. C. Xu, W. S. Oh, G. Liu, D. Y. Kim, D. W. Goodman, *J. Vac. Sci. Technol. A* **15**, 1261 (1997).
14. F. Pesty, H.-P. Steinrück, T. E. Madey, *Surfactant Sci.* **339**, 83 (1995).
15. S. D. Lin, M. Bollinger, M. A. Vannice, *Catal. Lett.* **17**, 245 (1993).

16. We acknowledge the support of this work by the Department of Energy, Office of Basic Energy Sciences, Division of Chemical Sciences, the Robert A. Welch Foundation, and the Dow Chemical Company. M.V. thanks the Academy of Finland for support as a Visiting Scientist.

7 May 1998; accepted 31 July 1998

Long-Range Electrostatic Trapping of Single-Protein Molecules at a Liquid-Solid Interface

Xiao-Hong Nancy Xu* and Edward S. Yeung†

The motion of single, dye-labeled protein molecules was monitored at various pH and ionic strengths within the 180-nanometer-thick evanescent-field layer at a fused-silica surface. Below the isoelectric point, molecules partitioning into the excitation region increased in number but maintained a random spatial distribution, implying that surface charge can influence the charged protein at distances beyond that of the electrical double-layer thickness. The residence times of the molecules in the interfacial layer also increased below the isoelectric point. However, immobilization on the solid surface for extended periods was not observed. Histograms of residence times exhibit nearly identical asymmetry as the corresponding elution peaks in capillary electrophoresis. These results are a direct verification of the statistical theory of chromatography at the single-molecule level, with the caveat that long-range trapping rather than adsorption is the dominant mechanism.

Insights into the detailed dynamics of adsorption and desorption at an interface are vital to designing new materials, elucidating biological processes at cell surfaces, studying electrochemical reactions, and understanding chromatographic mechanisms. For example,

in the statistical theory of chromatography, solutes freely diffuse in the mobile phase until they partition into the stationary phase, at which time their migration down the column is delayed. However, it has been difficult to establish how close molecules must approach a surface to be affected by its influence, whether and for how long molecules are immobilized, and to what extent individual retention events are truly random. Such questions can only be addressed by looking at single-molecule motion at realistic liquid-solid interfaces.

A variety of single-molecule studies have been performed in the liquid phase and studies have provided information, for example, on molecular sizes determined from fluorescence intensities (*1*), diffusion into and out of the confocal volume (*2, 3*), fluorescence correlation (*4*), reactivity by enzymatic amplification (*5–7*), motion in liquid bilayers (*8*) or in gel pores (*9*), reaction with an immobilized protein (*10*), and diffusion and photobleaching in free solution (*11*). In the last example, temporal resolution to 0.4 ms and spatial resolution to 0.3 μm were achieved by continuous imaging. Because the intensified charge-coupled device camera (ICCD) used in this previous and the present study is an integrating single-photon detector, the recorded spot size traces out the random-walk motion within the exposure time for molecules inside the excitation region [the evanescent-field layer (EFL)] (Fig. 1A).

Fluorescence from single molecules of concanavaline A conjugated with 5- (and 6-) carboxytetramethylrhodamine succinimidyl ester (ConA-TAMRA) was recorded at different solution pH. The protein concentration is low compared with the solution ionic strength to avoid interactions among protein molecules. We independently determined that the fluorescence properties of ConA-TAMRA are essentially constant (the intensity is within 20% with no spectral shift) under these buffer conditions. For pH > 4.3, a few molecules of the protein were recorded in the EFL, as expected (*12*). For pH < 4.3, there is a substantial increase in the number of molecules observed. The behavior follows a titration curve (Fig. 1B, blue triangles) with a break at pH 4.3, nearly identical to the isoelectric point (pI) of 4.5 for ConA. For the neutral dye molecule TAMRA (Fig. 1B, blue squares), a low count (mean = 8, σ = 46%) was observed throughout this pH range. Counts for TAMRA-labeled avidin (pI = 10) were higher (mean = 100, σ = 35%) but did not exhibit any sharp breaks in similar plots.

As molecules approach a solid surface from solution, the excitation intensity, and thus the fluorescence intensity, should increase exponentially (by a factor of 2.718 from the surface out to 180 nm, as depicted schematically in Fig. 1A) (*9*). From close examination of images like Fig. 2A, we found that the average intensity per pixel remains relatively constant for all molecules and for all pH conditions. Stochastic behavior within a factor of 2.718 around the average slopes in Fig. 2B is observed, characteristic of molecules randomly located inside the EFL rather than bunched together right at the solid surface.

The fused-silica surface contains ionizable silanol groups with a zeta potential of −0.25 mV at pH 6 (*13*), which decreases almost linearly to zero below pH 2 (potential of zero charge) (*14*). Above the pI, the negatively charged protein is expected to be repelled by the negatively charged surface. Below the pI, the protein is net positively charged and the surface is slightly negatively charged. Increased penetration of the protein into the interfacial region below pH 4.3 together with the decreasing number of molecules with the reduction of pH from pH 4 to pH 2.5 (Fig. 1B, blue triangles) are expected. What is not expected is that these surface effects occur at distances comparable with the EFL, which is 60 times the size of the charge interaction distance of 3 nm predicted by electrical double-layer models for these ionic strengths (*15–18*). The relative numbers of molecules (a quantity that is independent of intensities or spot sizes) as a function of pH in Fig. 1B and the random spatial distributions in Fig. 2B provide direct evidence for extended influence of the double layer. These observations help to explain several perplexing phenomena recently reported, such as reduced electroosmotic flow in capillary electrochromatography (*19, 20*), DNA size separation in free-zone electrophoresis (*21*), and abnormal electromigration of charged species in narrow channels (*22, 23*).

As the number of partitioned single-molecule spots increases toward lower pH, so do their sizes (Fig. 2B, blue symbols). The fraction of molecules exhibiting large sizes, not just their absolute numbers, increases at lower pH (Fig. 2C, blue symbols). There is evidence that molecular diffusion is actually slower near a surface (*11, 23*). Larger spot sizes therefore indicate longer residence times in the excitation region, that is, trapping within the EFL. The interfacial layer moves slower than the bulk (*24*) both in electromigration and in hydrodynamic flow, and thus trapping explains chromatographic retention of proteins on a fused-silica stationary phase (*25*). Contrary to the conventional picture of solutes coming on and off the stationary phase, we did not observe bright small spots in Fig. 2B that would result from actual immobilization for significant periods during exposure, thereby accumulating fluorescence photons in a small number of pixels. Just

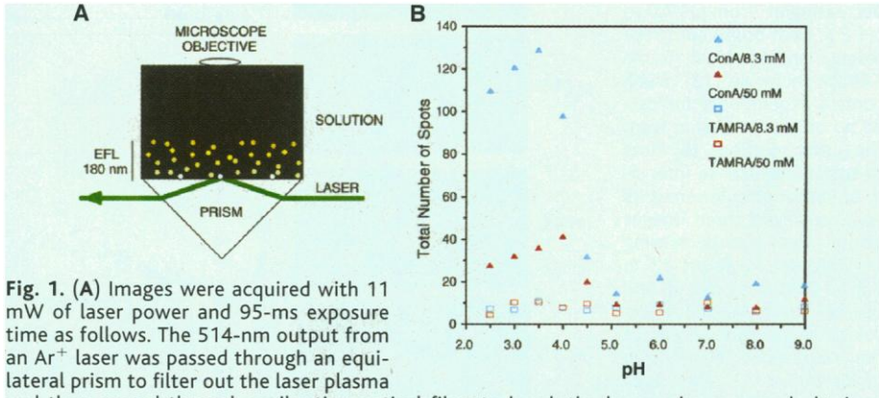

Fig. 1. (**A**) Images were acquired with 11 mW of laser power and 95-ms exposure time as follows. The 514-nm output from an Ar^+ laser was passed through an equilateral prism to filter out the laser plasma and then passed through a vibrating optical fiber to break the laser coherence and obtain a uniform beam. The unfocused output was passed through a beam expander and guided into an inverted fused-silica right-angle prism to create a total internal reflection elliptical spot (diameters: a = 1.4 cm; b = 0.3 cm) on the prism surface. The emission of molecules excited within the EFL was imaged with an ICCD (Princeton Instruments, ICCD-576 EMG/RB with ST-138 controller) through a ×100 microscope objective (numerical aperture = 1.3) directly immersed into the sample solution. A mechanical shutter was synchronized with the ICCD electronic shutter to minimize photobleaching by blocking the laser beam when data was not being collected. Good signal-to-noise ratio was achieved by carefully optimizing the laser excitation power and ICCD exposure time, and by using three consecutive interference filters (two 580-nm filters, 10-nm bandwidth, and one 560-nm long-pass filter) placed in front of the ICCD. (**B**) Plots of the numbers of molecules recorded versus pH for 100 nM ConA-TAMRA (blue triangles) [Molecular Probes, average conjugated molar ratio (F/p) = 3.4, or a protein concentration of 29 nM] and TAMRA (blue squares) in a 8.3-mM buffer solution, and ConA-TAMRA (red triangles) and TAMRA (red squares) in 50-mM buffer solution. Each data point represents the number of molecules accumulated from three independent measurements.

Ames Laboratory–U.S. Department of Energy and Department of Chemistry, Iowa State University, Ames, IA 50011, USA.

*Present address: Department of Chemistry and Biochemistry, Old Dominion University, Norfolk, VA 23529, USA.

†To whom correspondence should be addressed. E-mail: yeung@ameslab.gov

being in the proximity of the solid surface is sufficient for confinement or retention.

To correlate with chromatography, we performed capillary electrophoresis (CE) experiments on the same systems (Fig. 3). The capillary surface was fused silica, the identical material as the prism we used in imaging. It is known that in the absence of surface interactions CE peaks have a symmetrical Gaussian shape if the solute concentration is low (*26*). The finite peak width is due to axial diffusional broadening. TAMRA, which shows little partitioning in the EFL (Fig. 1B), gives a symmetrical peak in CE (Fig. 3A). ConA-TAMRA at pH 7 also shows negligible partitioning (Fig. 1B), and the CE peak remains quite symmetrical (Fig. 3B). At low pH, ConA-TAMRA partitions substantially into the EFL (Fig. 1B), and the CE peak shows significant tailing (Fig. 3C). The asymmetry of the peaks in Figs. 2C and 3 are strikingly similar over all buffer conditions. Figure 2C therefore validates the statistical theory of chromatography at the single-molecule limit.

To further elucidate the interaction mechanism between the surface and the protein, we performed identical experiments at higher ionic strengths, which should shield the net charge on the surface (decreasing the double-layer thickness) (*15–18*) and on the protein. We observed fewer molecules for ConA-TAMRA (Fig. 1B, red triangles) and a smaller number with long residence times (Fig. 2B, red symbols). The sharp transition at the pI and the decrease in numbers from pH 4 to pH 2.5 remain (Fig. 1B, red triangles). Because the thickness of the EFL should not change, these results depict a reduced efficiency for confinement of the protein by the fused-silica surface. CE at the higher ionic strength also shows a less distorted peak (Fig. 3D), which parallels the distribution in residence times

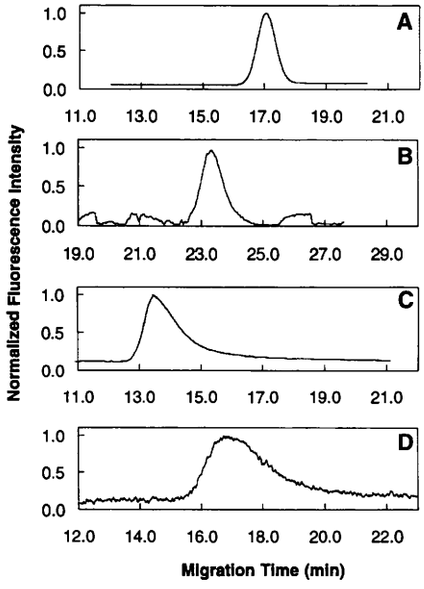

Fig. 3. Representative electropherograms of (**A**) TAMRA in 8.3-mM buffer at pH 3.2, (**B**) ConA-TAMRA in 8.3-mM buffer at pH 7.0, (**C**) ConA-TAMRA in 8.3-mM buffer at pH 3.2, and (**D**) ConA-TAMRA in 50-mM buffer at pH 3.2. Distortion parameters of the peaks were obtained by fitting the electropherograms with an exponentially modified Gaussian function. The normalized distortion parameters (d_p) were calculated by dividing the distortion parameter by the width of the peak The d_p for the peaks in (A) through (D) are 0.47, 1.2, 4.4, and 3.0, respectively. CE was performed in a bare fused-silica column with 75-μm internal diameter, 50-cm actual length, and 30-cm effective length by using laser-induced fluorescence detection excited by an unfocused 543.5-nm He-Ne laser beam (5 mW). The samples were introduced into the column with electrokinetic injection at 3 kV for 5 to 10 s, and the electrophoresis experiments were run at 10 kV. The concentrations of ConA-TAMRA and TAMRA were 600 nM (F/p = 3.4, or a protein concentration of 176 nM) and 100 nM, respectively. The bare column provided the same liquid-silica interface as the one created by the prism in Fig. 1A.

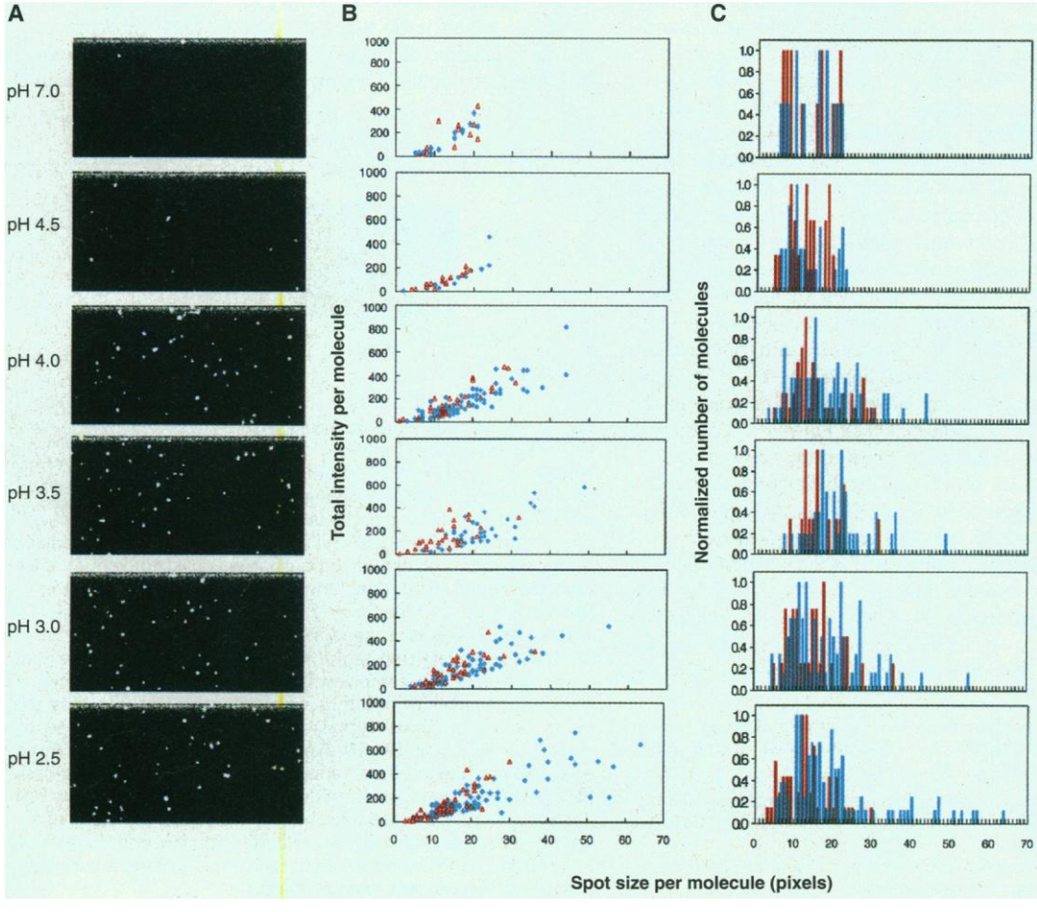

Fig. 2. (**A**) Representative images (100 by 200 pixels = 20 μm by 40 μm) of fluorescence at a liquid-silica interface from ConA-TAMRA in a 8.3-mM buffer solution at decreasing pH from pH 7.0 to pH 2.5. Each bright spot represents an individual ConA-TAMRA molecule (*12*). Blank control experiments indicated no obvious emission from the buffer solutions. (**B**) Plots of total fluorescence intensity of each molecule versus its spot size from three images similar to (A) at decreasing pH from pH 7.0 to pH 2.5 in 8.3-mM (blue symbols) and 50-mM (red symbols) buffer solutions. (**C**) Histograms of the normalized distribution of ConA-TAMRA spot sizes from three images similar to (A) at decreasing pH from pH 7.0 to pH 2.5 in 8.3-mM (blue symbols) and 50-mM (red symbols) buffer solutions.

(Fig. 2C, red symbols). We thus conclude that charge interaction is responsible for confinement of the protein.

Immobilization may be unfavorable because of steric effects or because proteins are not point charges. Our experiments show that molecules do not have to be physically immobilized to be chromatographically retained. Trapping is found in a thick zone where molecular behavior is intermediate between bulk and surface regimes. The large distances involved cannot be explained by the Derjaguin-Landau-Verwey-Overbeek theory (*27*) for interactions between charged surfaces across liquids, even in the regime of reduced charge densities (*28*). Long-range attractive interaction has been reported for polystyrene sulfonate spheres near a charged glass surface (*29*). The distances (50 nm if scaled to our ionic strengths) are comparable with those here, although metastable colloidal crystallites may not properly model proteins. It may well be that restricted motion of the counter ions near the surface (*11*) lowers the efficiency of electrostatic shielding to extend the interaction distance. This implies that the interaction of protein molecules with biological cell surfaces can be much more efficient than predicted by random diffusion, which in turn enhances binding to receptors. Although here we relied on the inherent surface charge on fused silica to follow one type of protein retention, other interactions can be studied by coating chromatographic materials, creating self-assembled monolayers, or attaching actual cell membranes on the solid surface.

References and Notes

1. J. T. Petty *et al.*, *Anal. Chem.* **67**, 1755 (1995).
2. S. Nie, D. T. Chiu, R. N. Zare, *Science* **266**, 1018 (1994).
3. ———, *Anal. Chem.* **67**, 2849 (1995).
4. M. Eigen and R. Rigler, *Proc. Natl. Acad. Sci. U.S.A.* **91**, 5740 (1994).
5. Q. Xue and E. S. Yeung, *Nature* **373**, 681 (1995).
6. W. Tan and E. S. Yeung, *Anal. Chem.* **69**, 4242 (1997).
7. D. B. Craig, E. A. Arriaga, J. C. Y. Wong, H. Lu, N. J. Dovichi, *J. Am. Chem. Soc.* **118**, 5245 (1996).
8. T. Schmidt, G. J. Schutz, W. Baumgartner, H. J. Gruber, H. Schindler, *Proc. Natl. Acad. Sci. U.S.A.* **93**, 2926 (1996).
9. R. M. Dickson, D. J. Norris, Y.-L. Tzeng, W. E. Moerner, *Science* **274**, 966 (1996).
10. T. Funatsu, Y. Harada, M. Tokunaga, K. Saito, T. Yanagida, *Nature* **374**, 555 (1995).
11. X.-H. Xu and E. S. Yeung, *Science* **275**, 1106 (1997).
12. These represent relative counts and not absolute counts, because the ICCD detection threshold was set artificially high to eliminate all false-positive events that would have distorted the accompanying measurements of spot sizes and to avoid artifacts due to photobleaching. Only the most extensively labeled molecules in the sample population can exceed the detection threshold. Their behavior is still representative because a neutral label is used.
13. J. C. Reijenga, G. V. A. Aben, Th. P. E. M. Verheggen, F. M. Everaerts, *J. Chromatogr.* **260**, 241 (1983).
14. W. J. Lambert and D. L. Middleton, *Anal. Chem.* **62**, 1585 (1990).
15. A. J. Bard and L. R. Faulkner, *Electrochemical Methods, Fundamentals and Applications* (Wiley, New York, 1980), pp. 488–510.
16. J. O'M. Bockris and A. K. N. Reddy, *Modern Electrochemistry* (Plenum, New York, 1970), vol. 2, pp. 826–841.
17. C. Gutierrez and C. Melendres, Eds., *Spectroscopic and Diffraction Techniques in Interfacial Electrochemistry* (Kluwer Academic, Boston, 1990), pp. 1–469.
18. J. Lipkowski and P. N. Ross, Eds., *Structure of Electrified Interfaces* (VCH, New York, 1993), p. 201 and p. 277.
19. T. S. Stevens and H. J. Cortes, *Anal. Chem.* **55**, 1365 (1983).
20. M. Martin and G. Guiochon, *ibid.* **56**, 614 (1984).
21. N. Iki, Y. Kim, E. S. Yeung, *ibid.* **68**, 4321 (1996).
22. J. Roeraade, Abstract WL-11-4, Eighth International Symposium on High Performance Capillary Electrophoresis, Orlando, FL, January 1996.
23. W. A. Lyon and S. Nie, *Anal. Chem.* **69**, 3400 (1997).
24. C. L. Rice and R. Whitehead, *J. Phys. Chem.* **69**, 4017 (1965).
25. D. A. Skoog and J. J. Leary, *Principles of Instrumental Analysis* (Saunders, New York, ed. 4, 1992), pp. 579–601.
26. F. E. P. Mikkers, F. M. Everaerts, Th. P. E. M. Verheggen, *J. Chromatogr.* **169**, 11 (1979).
27. B. V. Derjaguin and L. Landau, *Acta Physicochim. U.S.S.R.* **14**, 633 (1941); E. J. W. Verwey and J. Th. G. Overbeek, *Theory of the Stability of Lyophobic Colloids* (Elsevier, Amsterdam, 1948).
28. S. H. Behrens, M. Borkovec, P. Schurtenberger, *Langmuir* **14**, 1951 (1998). There, a secondary minimum is predicted as a result of the interplay between charge repulsion and van der Waals attraction. However, that feature is more prominent toward higher ionic strengths, in variance with our observations of enhanced trapping toward lower ionic strengths.
29. A. E. Larsen and D. G. Grier, *Nature* **385**, 230 (1997).

30. The Ames Laboratory is operated for the U.S. Department of Energy by Iowa State University under contract number W-7405-Eng-82. Supported by the Director of Energy Research, Office of Basic Energy Sciences, Division of Chemical Sciences.

26 January 1998; accepted 3 August 1998

Design of Organic Molecules with Large Two-Photon Absorption Cross Sections

Marius Albota, David Beljonne, Jean-Luc Brédas,* Jeffrey E. Ehrlich, Jia-Ying Fu, Ahmed A. Heikal, Samuel E. Hess, Thierry Kogej, Michael D. Levin, Seth R. Marder,* Dianne McCord-Maughon, Joseph W. Perry,* Harald Röckel, Mariacristina Rumi, Girija Subramaniam, Watt W. Webb,* Xiang-Li Wu, Chris Xu

A strategy for the design of molecules with large two-photon absorption cross sections, δ, was developed, on the basis of the concept that symmetric charge transfer, from the ends of a conjugated system to the middle, or vice versa, upon excitation is correlated to enhanced values of δ. Synthesized bis(styryl)benzene derivatives with donor-π-donor, donor-acceptor-donor, and acceptor-donor-acceptor structural motifs exhibit exceptionally large values of δ, up to about 400 times that of *trans*-stilbene. Quantum chemical calculations performed on these molecules indicate that substantial symmetric charge redistribution occurs upon excitation and provide δ values in good agreement with experimental values. The combination of large δ and high fluorescence quantum yield or triplet yield exhibited by molecules developed here offers potential for unprecedented brightness in two-photon fluorescent imaging or enhanced photosensitivity in two-photon sensitization, respectively.

In the presence of intense laser pulses, molecules can simultaneously absorb two or more photons, and the transition probability for absorption of two identical photons is proportional to I^2, where I is the intensity of the laser pulse. Molecules with a large two-photon absorption cross section, δ, are in great demand for variety of applications, including two-photon–excited fluorescence microscopy (*1*), optical limiting (*2*, *3*), three-dimensional optical data storage (*4*), and two-photon induced biological caging studies (*5*). These applications use two key features of two-photon absorption, namely, the ability to create excited states with photons of half the nominal excitation energy, which can provide improved penetration in absorbing or scattering media, and the I^2 dependence of the process, which allows for excitation of chromophores with a high degree of spatial selectivity in three dimensions through the use of a tightly focused laser beam. Unfortunately, most known organic molecules have relatively small δ, and criteria for the design of molecules with large δ have not been well developed (*6*, *7*). As a result, the full utility of two-photon–absorbing materials has not been realized. Here, we report on design strategies and structure-property studies for two-photon absorption, which resulted in the synthesis of fluorescent molecules with unprecedented δ values.